Applied Catalysis B: Environmental 140–141 (2013) 25–31

Contents lists available at SciVerse ScienceDirect

Applied Catalysis B: Environmental

journal homepage: www.elsevier.com/locate/apcatb

Electrical and catalytic properties of cerium–tin mixed oxides in CO depollution reaction

Anca Vasile [a], Veronica Bratan [a], Cristian Hornoiu [a,*], Monica Caldararu [a], Niculae I. Ionescu [a], Tatiana Yuzhakova [b], Ákos Rédey [b]

[a] Institute of Physical Chemistry "Ilie Murgulescu", Romanian Academy, Splaiul Independentei 202, 060021 Bucharest, Romania
[b] Institute of Environmental Engineering, University of Pannonia, 10. Egyetem Str, Veszprém 8200, Hungary

ARTICLE INFO

Article history:
Received 4 December 2012
Received in revised form 23 March 2013
Accepted 27 March 2013
Available online 2 April 2013

This article is dedicated to the memory of Dr. Monica Caldararu.

Keywords:
Tin–cerium mixed oxides catalysts
Electrical conductivity
Surface dynamics
CO oxidation

ABSTRACT

AC electrical conductivity of CeO_2 catalyst samples containing 5, 10 and 20 wt% SnO_2 prepared by co-precipitation and of SnO_2 and CeO_2 pure oxides (prepared under the same conditions) was measured in *operando* conditions. The measurements were carried out at a frequency of 1592 Hz in the temperature range from room temperature up to 400 °C, using successively programmed heating–cooling cycles under various atmospheres. The catalyst samples were tested in the catalytic oxidation of CO in presence and in absence of oxygen in the same temperature range (30–400 °C). An improved deep oxidation of carbon monoxide has been found with these co-precipitated mixed oxides compared to pure components, leading to a better catalytic activity at lower temperature. The band gap energies were estimated based on the UV–Vis spectra and correlated with XRD results and AC electrical conductivity data. These results show the influence of the tin oxide on the electrical properties and oxygen mobility of the catalytic systems studied and on the surface behaviour of ceria.

1. Introduction

In the last time several papers [1–6] have dealt with the behaviour of ceria based mixed oxide catalysts in catalytic oxidation reactions. One of the conclusions of these studies was the existence of a synergetic effect in the redox properties of the constituents. Some of the ceria based mixed oxides were found to exhibit a better catalytic properties in comparison with the parent pure oxides and an increase the oxygen storage/release capacity.

CeO_2 is a commonly used component of the three-way catalysts used for the elimination of toxic substances such as CO, VOC, C_nH_m, NO_x from the exhaust gases of the vehicles [7]. One of the important properties of ceria in terms of using it in catalysis is its oxygen storage capacity (OSC), since it acts as an oxygen reservoir regulating the partial pressure of oxygen near the catalyst surface [7,8] and provide oxygen to the gas mixture. The key factor regarding this property is the reversible transformation from Ce^{4+} to Ce^{3+} resulting in the formation of oxygen vacancies (coordinatively unsaturated sites) on the cerium oxide surface. The redox properties of the ceria and the high mobility of the lattice oxygen were generally considered to be the principal factors in governing the catalytic behaviour in oxidation reactions.

The transition metal oxides have multivalent oxidation states that allow the material to easily donate lattice oxygen to react with the adsorbed molecules, the catalytic surface being subsequently re-oxidized by the gas-phase oxygen. In this way, on these oxide catalysts the oxidation reactions are supposed to follow the Mars–van Krevelen mechanism, according to which the molecules are oxidized by consuming lattice oxygen of the oxide catalyst which in turn is re-oxidized by gas-phase oxygen. The effects of oxidation–reduction cycle of the catalytic system can be followed by measuring the surface conductivity. SnO_2 is frequently used among the oxides as a material for sensors and as a component of oxidation catalysts; however, its activity and electrical response to the ambient conditions are limited by its low surface area (only several m^2/g). It was shown that the doping SnO_2 with rare earth oxides into influences the catalytic properties of SnO_2 due to their acid/base characteristics [9–14].

The aim of this paper was to study the influence of the combination of increasing amounts of SnO_2 on ceria in order to identify the relationship between the redox behaviour as resulted from electrical measurements and their catalytic performances in CO oxidation reaction. In addition the catalytic test of CO oxidation without oxygen was performed in order to study ability of oxygen storage capacity of mixed oxides and its surface/bulk mobility.

* Corresponding author. Tel.: +40 21 3121147; fax: +40 21 3121147.
E-mail address: chornoiu@icf.ro (C. Hornoiu).

0926-3373/$ – see front matter © 2013 Elsevier B.V. All rights reserved.
http://dx.doi.org/10.1016/j.apcatb.2013.03.042

2. Experimental

2.1. Catalyst preparation

The SnO_2–CeO_2 catalyst samples (with a content of 5, 10 and 20 wt% SnO_2) were obtained by mixing aqueous solutions of tin (II) dichloride dehydrate ($SnCl_2{\cdot}2H_2O$, >99%, Interkemia) and cerium (IV) ammonium nitrate ($(NH_4)_2Ce(NO_3)_6$, 99+%, Merck). Co-precipitation was achieved by addition of ammonium hydroxide. A similar procedure was used for obtaining pure SnO_2 and CeO_2 from the same precursors. The preparation of the catalyst samples was previously given [15]. The catalyst samples obtained were labelled as follows: Sn5–Ce for the sample containing 5 wt% of SnO_2, Sn10–Ce and Sn20–Ce for samples with 10 and 20 wt% tin oxide content, respectively.

2.2. Characterization

The surface properties of the prepared oxides were investigated and the results of UV–Vis, electrical conductivity and catalytic activity measurements in CO oxidation reaction by reactants conversion measurements are presented. The crystalline structure was examined by X-ray diffraction (XRD). The experimental data obtained were correlated with the results of BET surface area and acidity measurements carried out previously on the same catalysts [15].

Diffuse reflectance UV–Vis spectra in the 900–200 nm range were obtained using a Perkin Elmer, Lambda 35 spectrophotometer operating at room temperature and using spectralon as a standard.

AC electrical conductivity measurements were carried out in a cell consisting of two coaxial tantalum cylinders as electrodes embedded in a Pyrex glass tube. This cell was specially designed to allow simultaneous electrical and catalytic activity measurements in powders under *operando* conditions [16–18]. The sample powder (fraction between 0.25 and 0.5 mm) was placed in the annular space between the electrodes and supported on a frit. The electrical conductivity (σ) of the powder bed was measured at 1592 Hz, in gas flow with a RLC bridge (HIOKI 3522-50) by using the differential step technique (DST) described previously [16–18]. At this frequency it was concluded that the conductivity of the powder was dominated by surface conduction [19]. These AC measurements were used also for catalytic materials [19–22], the model being the Schottky barrier controlled conductivity [23].

The measurements were performed by successive thermal cycling, namely heating ($2^\circ/5^\circ$C min^{-1} heating rate between room temperature and 400 °C) – cooling (about 10 °C min^{-1} cooling rate) cycles, and changing the gases according to the protocol described below:

$$\text{DHe(1–3)} \rightarrow \text{DO} \rightarrow \text{DHe4} \rightarrow \text{CT1} \rightarrow \text{DHe5} \rightarrow \text{CT2} \rightarrow \text{DHe6}$$

where DHe – dry helium (the numbers given above indicate the cycle number), DO – dry oxygen, CT1 – CO:O_2:He (5:5:90), CT2 – CO:He (5:95). Before each heating run, the sample was flushed for 30 min with the corresponding gas mixture at room temperature. Cooling was done in the same gaseous atmosphere, then the cell was closed and the sample was kept overnight in the same atmosphere. The measurements were coupled with the permanent monitoring of the composition of the inlet/outlet gas by on-line gas chromatography. The overall flow rate in all cases was 72 mL min^{-1}. Dry gases (except gas mixtures) were obtained by passing the research grade compounds through molecular sieves units.

2.3. Catalytic tests

The catalytic activities of the samples were studied in CO oxidation reactions according to the differential step technique (DST) protocol [16–18]. The effluent was periodically analysed by gas chromatograph. The exit gas analysis was performed with a GC (Pye, TCD detector) attached on-line and equipped with molecular sieves 5 Å column with helium as carrier gas. CO oxidation was performed in a mixture of CO:O_2 (1:1) balanced with helium (i.e. CO:O_2:He 5:5:90). Ratio CO:He (5:95) was used for CO oxidation run without oxygen in order to check the activity and mobility of lattice oxygen.

3. Results and discussion

The results on elements distribution of the SnO_2–CeO_2 samples studied using surface mode analysis evidence their relatively homogeneous distribution in the near-surface layer of the catalyst. The weight percent of elements was closed to the calculated one used for preparation of samples and also indicates presence of Cl in the surface layer of sample: 0.30 wt% for SnO_2 sample and 0.42 wt% for Sn20–Ce sample. The presence of Cl detected in the SnO_2 and Sn20–Ce samples originates from the solution of $SnCl_2{\cdot}2H_2O$ used for the preparation of samples by co-precipitation method and from impurities of $(NH_4)_2Ce(NO_3)_6$ salt (max 0.001%). The increase of surface area can be obtained by the precipitation method of preparation using nitrate compounds [10–12]. One of good thing of using nitrates is that those compounds are easily decomposed at temperatures 230–250 °C [12] without harmful deposition at catalytic surface.

The catalysts samples have been primary characterized [15]. The acidic sites, which were detected on the surface of SnO_2–CeO_2 mixed samples and pure samples, might be directly involved in CO (a weak base) oxidation. It is interesting to note that the mixed oxides have a surface area two or more time bigger than the main component CeO_2 (46 m^2/g) and seven or more time than second component SnO_2 (13 m^2/g) (see Table 1), suggesting the high dispersion of the oxides which occurs as a result of the simultaneous precipitation (i.e. co-precipitation) of the oxides and which has been proved by Scanning Electron Microscope [15]. It can be seen (Table 1) that S_{BET} of mixed oxides depends on the tin oxide loading. The surface area decreases with the increase amount of SnO_2.

The XRD sharp peaks obtained for SnO_2 corresponded to a mixture of cassiterite (tetragonale) and orthorhombic structure of SnO_2. For pure ceria and for mixed oxides the XRD pattern showed the diffraction lines of cerianite crystallite having fluorite structure (as identified using the standard data JCPDS 34-0394) responsible for the unique properties of ceria to release and uptake oxygen under different conditions; the crystallinity of ceria decreases with increasing of the SnO_2 loading. No separate tin oxide structure was observed for SnO_2–CeO_2 samples. Commercial cerium (IV) oxide ($CeO_2 \sim 99.9\%$, Sigma, fine powder) was used as reference sample for calculation of crystalline size, lattice strain and lattice parameters of co-precipitated samples. The crystalline size of samples decreases with the increasing of the SnO_2 loading and with the decreasing of ceria crystallinity.

For the studied samples the lattice strain, *e*, value increases with increasing of the SnO_2 loading. Generally lattice strain arises from displacements of the unit cells from their normal positions which can be produced by surface restructuring, lattice vacancies, dislocations or substitution of atoms in the crystalline cell unit.

Using UV–Vis spectra, the band gap energy of metal oxides can be calculated. The electrical conductivity measurements presented below showed that the conductivity exhibited on mixed oxides follows the pattern of the dominant ceria matrix. This behaviour is

Table 1
The abbreviations, BET surface area, crystalline size, lattice parameters and lattice strain of the investigated materials (fresh samples).

Samples	Abbreviation	BET surface area (m^2/g)	Crystalline size, D (Å)	Lattice parameter, $a \pm$ error (Å)	Lattice strain, e (%)
CeO_2 reference	–	–	–	5.41130	–
CeO_2	CeO_2	46	149	$5.41841 \pm 0.156 \times 10^{-2}$	1.293
5% SnO_2/CeO_2	Sn5–Ce	105	75	$5.41290 \pm 0.172 \times 10^{-2}$	2.241
10% SnO_2/CeO_2	Sn10–Ce	99	63	$5.40909 \pm 0.227 \times 10^{-2}$	2.602
20% SnO_2/CeO_2	Sn20–Ce	93	43	$5.39783 \pm 0.104 \times 10^{-2}$	3.612
SnO_2	SnO_2	13	–	–	–

confirmed also by the variation of the band gap energy calculated based on the UV–Vis spectra, which were recorded before and after the thermal cycling procedure. The band gap energy is a major factor determining the electrical conductivity and the Fermi level of a solid semiconductor metal oxide. The energy dependence of the absorption coefficient (α) for semiconductors in the region near the absorption edge is given by:

$$\alpha \sim \frac{(h\nu - E_0)^{\eta}}{h\nu} \quad (1)$$

where $h\nu$ is the energy of the incident photon and E_0 is the optical absorption edge energy; the exponent η depends on the type of optical transition caused by photon absorption [24]. In crystalline semiconductors η is 1/2, 3/2, 2 and 3 when the transitions are direct-allowed, direct-forbidden, indirect-allowed and indirect-forbidden, respectively. With an appropriate choice of η, a plot of $(\alpha h\nu)^{1/\eta}$ vs $h\nu$ is linear near the edge and the intercept of the line on the abscissa (at $(\alpha h\nu)^{1/\eta} = 0$) gives the optical absorption edge energy E_0. The Kubelka–Munk function ($F(R_\infty)$), where R_∞ is the reflectance for an infinitely thick sample, was used to convert the diffuse reflectance data into the absorption spectra. Then a plot of $((F(R_\infty)\cdot h\nu)^{1/\eta}$ vs. $h\nu$ can be used to determine the optical absorption edge energy E_0. The band gap energies values obtained considering direct-allowed transitions ($\eta = 1/2$) are presented in Table 2.

The value obtained for SnO_2 is smaller than the value reported in the literature (3.6 eV) [25]. This can be due to the presence of defect sites, i.e. oxygen vacancies and possibly Sn^{2+} ions formed during reduction step of CO_2 desorption [26]. The data presented in Table 2 show that increasing SnO_2 content, the band gap energy values obtained for mixed oxides are decreasing, in concordance with the XRD results (the crystallinity of ceria decreases with increasing of SnO_2 loading). The lattice parameter decreases with the substitution of Ce^{4+} ($r = 0.97$ Å) by Sn^{4+} ($r = 0.71$ Å) due to the lattice shrinkage and distortion [27]. This may be an indication that SnO_2 could be incorporated into the CeO_2 lattice because Sn^{4+} is smaller than Ce^{4+}, reflecting the contraction of the ceria crystal lattice, and/or the formation of oxygen vacancies. Substitution of Sn^{4+} into CeO_2 lattice could induces formation of intermediate energy levels in the CeO_2-semiconductor on sides of Fermi level that cause a change in the band gap [28]. There are only small differences in the band gap energies values between the fresh and used samples indicating that the samples are quite stable in their initial state.

The investigations on the electrical and catalytic properties of the SnO_2–CeO_2 catalysts and of their component single oxides were performed under *operando* conditions. The electrical properties of semiconductor oxide powders are determined by the transport of carriers over the Schottky-type barriers at the contacts between the adjacent grains. Surface reduction/oxidation, hydration/dehydration and/or adsorption/desorption/reaction are reflected in the topography of inter-grain areas and thus in the height of inter-grain Schottky-type barriers. The corresponding modification of the nature and mobility of the surface dipoles results in changes in the electric properties of the surface layer [29]. A joint effect of the reaction gas mixtures and temperature on the topography of the grain surface and on the inter-grain barrier heights can be observed. So it is possible to follow the dynamics of gas–surface interactions, e.g. to monitor the changes in the oxidation states of the catalysts surfaces under reaction conditions [16,18,30–33]. It is known that for n-type semiconductors, oxygen adsorption must be associated with a decrease of conductivity due to the electron trapping by the oxygen adsorbed species while the loss of oxygen by repeated inert flushing is equivalent with a slight reduction, which must induce an increase in conductivity. The electrons and vacancies can be provided by the following reactions:

$$O_O^{*} \leftrightarrow V_O^{*} + 1/2O_{2(g)} \quad (2)$$

$$V_O^{*} \leftrightarrow V_O^{\bullet} + e^{-} \quad (3)$$

$$V_O^{\bullet} \leftrightarrow V_O^{\bullet\bullet} + e^{-} \quad (4)$$

where O_O^{*} is the lattice oxygen and V_O^{*}, $V_O^{\bullet}$, $V_O^{\bullet\bullet}$ are the neutral, singly or doubly ionized oxygen vacancies. The samples behave as

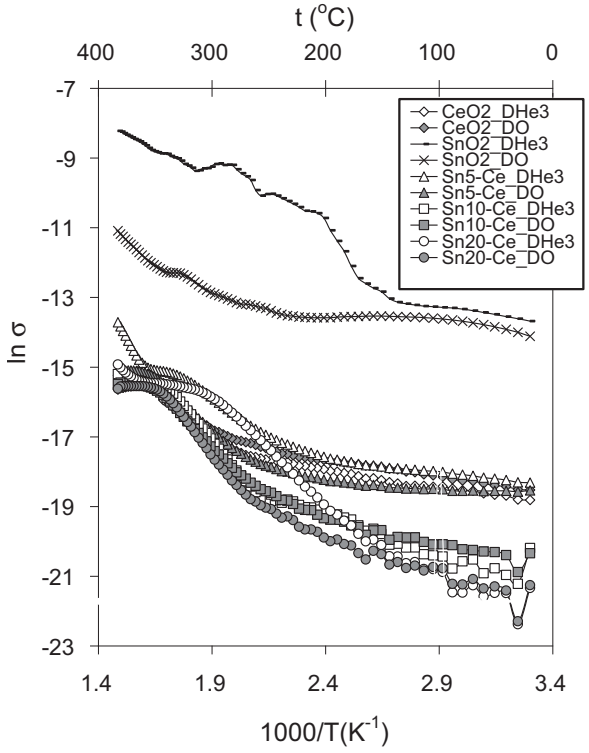

Fig. 1. Temperature dependence of electrical conductivity, σ (S/m), measured in *operando* conditions for SnO_2, CeO_2 and 5, 10, 20% SnO_2/CeO_2 samples in dry helium (DHe3) and in dry oxygen (DO).

Table 2
Band gap energies from UV–Vis data of fresh and used samples.

Band gap energy (eV)	SnO_2	CeO_2	Sn5–Ce	Sn10–Ce	Sn20–Ce
Fresh samples	3.28	3.19	3.05	3.02	2.97
Used samples	3.23	3.16	3.07	3.04	3.02

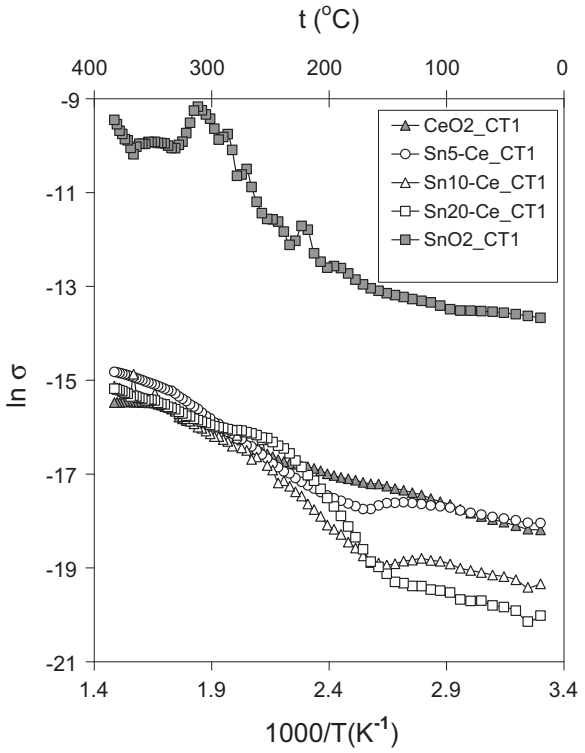

Fig. 2. Arrhenius plots for the variation of electrical conductivity σ (S/m) on progressive heating of SnO_2, CeO_2 and 5, 10, 20% SnO_2/CeO_2 samples in CT1 run (CO:O_2 1:1).

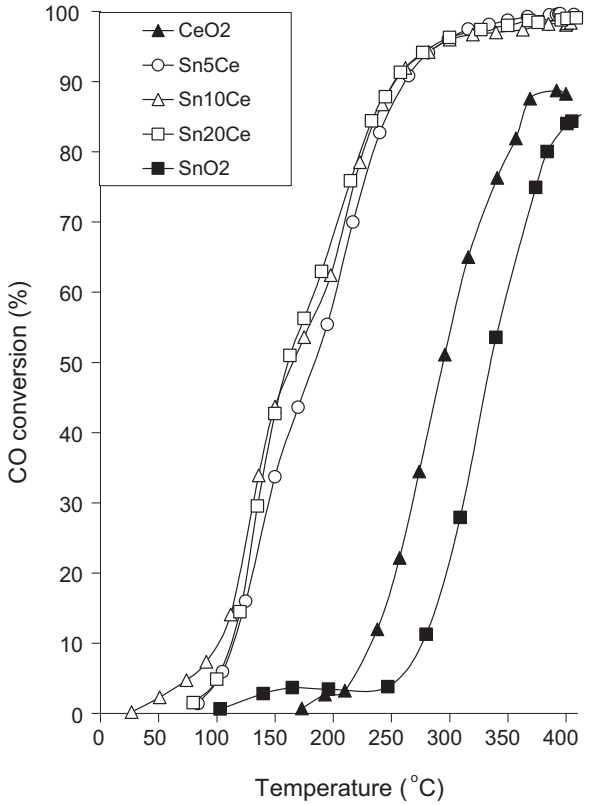

Fig. 3. Conversion-temperature dependence of SnO_2, CeO_2 and 5, 10, 20% SnO_2–CeO_2 samples in CO oxidation reaction in presence of oxygen (CT1 run).

an n-type semiconductor in the temperature range of 30–400 °C (Fig. 1).

Lower conductivity can be observed in oxygen atmosphere and higher conductivity can be seen in inert atmosphere. The SnO_2 sample exhibits a much higher conductivity values. Moreover, the n-type behaviour is more obvious for this sample. Significant decrease in conduction can be observed in the presence of oxygen (DO run) in case of SnO_2 sample than for the other catalyst samples, suggesting the presence of a higher number of oxygen vacancies on the SnO_2 sample surface. The same effect can be observed in case of the sample with the highest tin oxide content, Sn20–Ce. The conductivity behaviour of ceria containing samples follows the pattern of the dominant ceria matrix (lower conductivity); for Sn20–Ce sample, a steep increase in the conductivity was observed in the low temperature range, facilitated by the presence of weakly adsorbed water/OH groups on SnO_2 and CeO_2 surfaces and their higher mobility [18,32].

Fig. 2 shows the variation of electrical conductivity with temperature for all catalyst samples during heating in the presence of oxygen in the feed, i.e. CT1 run. In this run the SnO_2 sample exhibits also a much higher conductivity values than other samples. The conductivity values and the general behaviour of the mixed oxides are governed by the dominant matrix of CeO_2.

However, for the Sn10–Ce and Sn20–Ce samples, the conductivity variation with temperature between 125 and 250 °C (2.5–1.9 1000/K^{-1}) is steeper. For mixed oxides the two main parts of the Arrhenius plots can be observed: up to approximately 100 °C (2.68 1000/K^{-1}) a slight increase of conductivity and after 100 °C, up to 400 °C (1.48 1000/K^{-1}) a more pronounced increase of conductivity. The plots obtained in CT1 run show a progressive conductivity increase above 100 °C, suggesting a lattice mobilization with the temperature increase. The conductivity increase around 100 °C is in relation with the sharp increase of the CO conversion to CO_2 for mixed oxides (Fig. 3).

The conversion curves exhibited in CO oxidation for mixed oxides, i.e. CT1 run (Fig. 3) passes from the kinetic regime in the low temperature range in the diffusion regime at higher temperatures (i.e. ~300–400 °C). In the diffusional regime, the reaction rate is limited by the mass transfer between catalyst and flowing gas mixture. The obtained results prove also the reversibility of the surface reduction/oxidation level. The catalytic tests were relatively shorts, so a surface over-reduction for long-term catalytic reaction was not observed.

The conductivity of polycrystalline semiconductor metal oxides reflects a combination of bulk, grain-boundary and surface properties [23]. The first is also thermally activated; the surface conductivity may be increased or decreased by the substrate. The increase of conductivity above 100 °C (Fig. 2) indicates an increase of charge carriers density at the surface above this temperature that could be given by the adsorption of CO (soft base molecule). The nature of the oxygen surface species depends on the temperature, i.e. oxygen adsorbs on solid surface non-dissociatively in a molecular form (either neutral $O_{2(ads)}$ or charged $O_2{}^-{}_{(ads)}$) at lower temperatures (<150–200 °C), and at higher temperatures it dissociates into atomic oxygen (either neutral $O_{(ads)}$ or charged $O^-{}_{(ads)}$ or $O^{2-}{}_{(ads)}$). The main active species in the catalytic reaction could be the lattice oxygen. This can suggest a catalytic system according to Mars–van Krevelen mechanism. The following reaction scheme provides a simplified and generalized representation of CO and O_2 adsorption/desorption on catalysts surface.

$$1/2O_{2(gas)} \rightarrow O_{(ads)} \quad (5)$$

$$O_{(ads)} + e^- \rightarrow O^-{}_{(ads)} \quad (6)$$

$$CO_{(ads)} + O^-{}_{(ads)} \rightarrow CO_{2(gas)} + e^- \quad (7)$$

or

$$1/2O_{2(gas)} \rightarrow O_{(ads)} \quad (8)$$

$$1/2O_{(ads)} + e^- \rightarrow O^-_{(ads)} \quad (9)$$

$$O^-_{(ads)} + e^- \rightarrow O^{2-}_{(ads)} \quad (10)$$

$$O^{2-}_{(ads)} \leftrightarrow O^{2-}_{(lattice)} \quad (11)$$

$$CO + O^{2-}_{(ads)} \rightarrow CO_2 + 2e^- \quad (12)$$

It should be noted that the ceria containing tin oxide catalyst is able to convert CO to CO_2 at temperatures below 100 °C contrary to pure CeO_2 and SnO_2 which start to be active only at higher temperatures above 200 °C (Fig. 3). The CO conversion during CO oxidation, in presence of oxygen, is reached 50% at ~150 °C and exhibits higher values over mixed oxides than that over component oxides at about 400 °C (88.7% over CeO_2 and 84.0% over SnO_2). Mixed oxides exhibit maximum CO conversion 99.6% over Sn5–Ce, 98.1% over Sn10–Ce and 99.0% over Sn20–Ce at about 400 °C in CO oxidation to CO_2 reaction. One reason could be that mixed oxides have from two to seven times higher surface areas in comparison with CeO_2 and SnO_2, respectively. On the other hand XRD result shows that the crystallinity of ceria decreases with increasing of SnO_2 loading [28] which might generates a more defected lattice having higher lattice oxygen activity. Their activity seems to be mainly related to two factors: oxygen storage/redox capacity and surface area. The surface area is not the dominant factor in the controlling the activity but the concentration of active sites exposed to the reaction interface must be also considered. The mobility of oxygen released from SnO_2–CeO_2 might be another factor that influences the CO oxidation.

The Arrhenius plots for catalyst samples studied in a reducing atmosphere, i.e. CO:He mixture (CT2 run), are presented in Fig. 4. All the samples were very sensitive to the presence of CO in absence of oxygen. A very sharp increase in the conductivity values indicates adsorption of CO (supplier of electrons to surface) and/or a surface reduction. The surface reduction means the consumption of surface lattice/bulk oxygen under these conditions.

The order of magnitude increase in conductivity and thus in the level of surface reduction and the measured values of surface conductivity exhibited at 400 °C in CT2 run and in previous heating cycle, DHe5 run, are presented in Table 3.

Using the conductivity values for mixed oxides by flushing in inert atmosphere (i.e. DHe5 run) as a reference one can observed the enhancement of the conductivity by flushing a reducing atmosphere (i.e. CT2 run); the order of magnitude decreases in the following order: Sn5–Ce > Sn10–Ce > Sn20–Ce. In terms of the reduction level the obtained data suggest a stabilizing effect of the tin oxide on cerium oxide under reducing conditions.

The catalytic activity of CO oxidation was also followed in absence of oxygen (CT2 run), when CO_2 was obtained as a product, indicating that the lattice oxygen is involved in the CO conversion (Fig. 5).

Table 3
The measured values of surface electrical conductivity, σ (S/m), in DHe5 and CT2 run, at 400 °C.

Samples	σ_{DHe5} (S/m)	σ_{CT2} (S/m)
CeO_2	1.73×10^{-7}	6.37×10^{-4}
Sn5–Ce	2.92×10^{-7}	29.76×10^{-4}
Sn10–Ce	2.56×10^{-7}	2.90×10^{-4}
Sn20–Ce	3.31×10^{-7}	8.41×10^{-5}
SnO_2	2.02×10^{-4}	6.19×10^{-4}

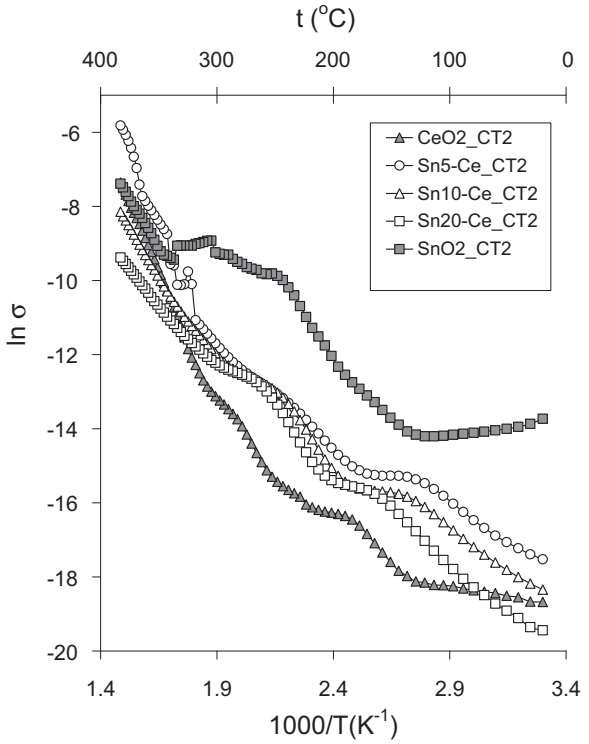

Fig. 4. Arrhenius plots for the variation of electrical conductivity σ (S/m) of SnO_2, CeO_2 and 5, 10, 20% SnO_2–CeO_2 samples on progressive heating in CO in absence of oxygen (CT2 run).

In this case the conversion of CO to CO_2 is a measure of the sample ability to release oxygen in absence of gaseous O_2. It is interesting to be noted that after a certain temperature, around 250 °C, the amount of CO_2 formed decreases indicating that the surface is excessively reduced and cannot provide anymore the necessary lattice oxygen (Fig. 5). The onset temperature for CO transformation is lower for mixed oxides than that for ceria under the reaction conditions. As shown in Fig. 5, the onset of the oxidation activity for mixed oxides was detected around 100 °C (with low conversion to CO_2). The mixed oxides catalysts exhibited higher CO conversion values at 400 °C (17.2% over Sn5–Ce, 25.8% over Sn10–Ce and 40.0% over Sn20–Ce) than conversion values exhibited at the same temperature over single oxides (only 2.3% over CeO_2 and 5.3% over SnO_2). Since no molecular oxygen exists during the measurement in CT2 run, the CO_2 should be produced by the reaction of CO with the oxygen released from the surface of the oxides; the formation of oxygen vacancies improves the mobility of lattice oxygen. This also supports the existence of a surface reduction indicated by the conductivity results. In the experiment performed in absence of oxygen (CT2 run) the conductivity presents an enhancement both before and after the onset temperature of oxidation activity (around 100 °C), the increase of conductivity evidenced for SnO_2–CeO_2 samples even before the onset of reaction (see Fig. 4) has indicated that the increase in charge carriers density is not enough for the catalytic activity. In Fig. 4 mainly three reduction ranges could be noticed for the studied samples: (i) low temperature range, up to approximately 120 °C – could be associated with CO adsorption on surface; (ii) between 120 and 210 °C – consumption of surface oxygen during reaction and activation of lattice oxygen involved in CO oxidation reaction by the temperature increase (iii) above 210 °C – lattice oxygen probably originated from deeper bulk layers can be involved.

In order to have a better understanding regarding the conduction process and the change in conductivity related with the

Table 4
The apparent activation energy of conduction estimated in the temperature range 300–400 °C.

Sample	$E_{a\,(CT1)}$ (eV)	$E_{a\,(CT2)}$ (eV)
CeO_2	0.04 ± 0.01	1.27 ± 0.06
Sn5–Ce	0.15 ± 0.02	1.43 ± 0.02
Sn10–Ce	0.16 ± 0.02	0.91 ± 0.06
Sn20–Ce	0.14 ± 0.02	0.67 ± 0.04
SnO_2	0.74 ± 0.03[a]	0.69 ± 0.03

[a] E_a were determined in the temperature range 365–400 °C.

progressive loading of SnO_2 to CeO_2, the apparent activation energy of conduction was estimated from the slope of $\ln(\sigma)$ vs $1/T$ plots obtained in the two heating runs CT1 and CT2, respectively, in the temperature range 300–400 °C (see Figs. 2 and 4) and are summarized in Table 4.

In case of CO oxidation reaction in presence of oxygen (CT1 run) the addition of tin dioxide to ceria produces an increase of the apparent activation energy of conduction. The values exhibited for mixed oxide catalysts do not vary significantly (from 0.14 to 0.16 eV) and are more appropriate to the apparent activation energy of CeO_2 (0.04 eV), indicating the important role of ceria. The SnO_2 sample exhibited higher apparent activation energy value (0.74 eV) compared to ceria and mixed oxides. This could be an indication that the number of active sites on tin dioxide surface is much more limited for CO oxidation, in presence of oxygen, in comparison with other samples due to its lowest surface area (Table 1), the pure SnO_2 having the lowest catalytic activity in CT1 run (Fig. 3).

Under reducing atmosphere (CT2 run) the addition of 5% of tin oxide to ceria has the effect of an increase of E_a. On increasing the tin oxide loading a decrease in the apparent activation energy value can be observed. By adding 5–20% SnO_2 on CeO_2, the reduction of apparent activation energy for conduction values from 1.43 to 0.67 eV indicates an enhancement of the mobility of the oxygen vacancies, in agreement with catalytic test data where Sn20–Ce has the highest activity in CT2 run in the high temperature range 300–400 °C (Fig. 5).

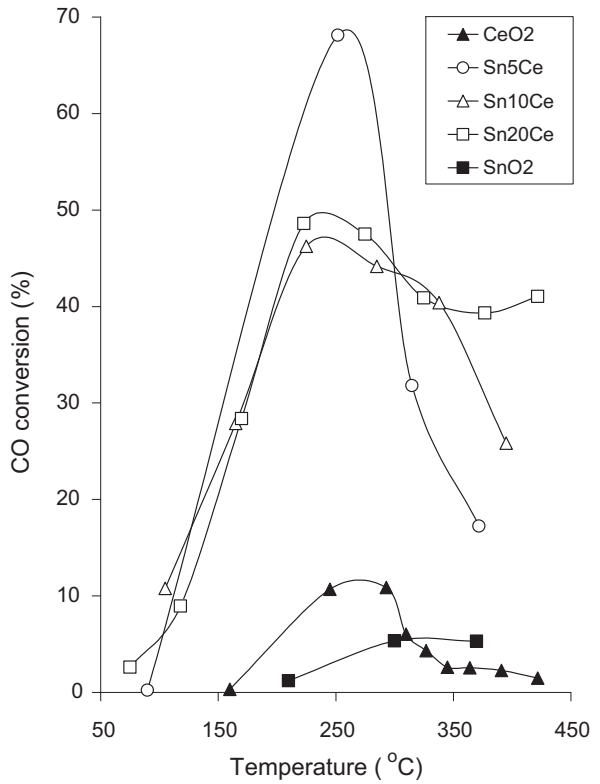

Fig. 5. Conversion-temperature dependence for SnO_2, CeO_2 and 5, 10, 20% SnO_2–CeO_2 samples in CO oxidation reaction in absence of oxygen (CT2 run).

The electrical conductivity is simultaneously determined by the concentration of charge carriers (electron/hole) and their mobility. There is no direct connection between the apparent activation energy of conduction and the catalyst activity, but the activation energy may be related to a variation of the energy of formation of defects that could significantly influence the catalytic behaviour of mixed oxides.

The simultaneous effects of the temperature and atmosphere make the interpretation of conductivity data very complex. One can obtain valuable information on the evolution of the catalyst surface under reaction conditions, but from the measurement data obtained in operando conditions one can see only a global phenomenon effect regarding the changes produced by adsorption/desorption/reaction, a sum of processes that occur involving CO adsorbed, oxygen lattice, oxygen vacancies and their mobility on the catalyst surface or diffusion of oxygen from the bulk to the surface lattice of mixed oxides, processes that one cannot yet distinguish.

4. Conclusions

The reaction of CO oxidation on Ce–Sn mixed oxides and on pure components CeO_2 and SnO_2 was investigated. Based on electrical conductivity measurements, BET, XRD, UV–Vis data and catalytic tests it results that ceria influences the physico-chemical properties of mixed oxide in a higher extent than tin dioxide. At the same time the catalytic activity of ceria and tin dioxide is improved by the mixing together these oxides and the reaction temperature in CO oxidation reaction is lowered.

The electrical conductivity data showed the n-type semiconductor behaviour for all samples. Following the dynamics of gas–surface interaction in terms of relative surface oxidation level, informations about the factors that influence the catalytic behaviour in this case, namely oxygen storage/redox capacity and mobility of oxygen lattice/oxygen vacancies were obtained.

The reaction mechanism of CO oxidation to CO_2 is similar in presence or in absence of oxygen in the feed and could be assimilated to a Mars–van Krevelen mechanism.

Acknowledgements

This research was carried out within the frame of the Agreement for Scientific and Educational Cooperation between the University of Pannonia, Veszprém, Hungary and the Institute of Physical Chemistry, "Ilie Murgulescu", Romanian Academy, Bucharest, Romania. This article was made under the projects TÁMOP-4.2.1/B-09/1/KONV-2010-0003 and TÁMOP-4.2.2/B-10/1-2010-0025 supported by the European Union and co-financed by the European Social Fund.

References

[1] A. Boffa, C. Lin, A.T. Bell, G.A. Somorjai, Journal of Catalysis 149 (1994) 149–158.
[2] A.P. Maciel, P.N. Lisboa-Filho, E.R. Leite, C.O. Paiva-Santos, W.H. Schreiner, Y. Maniette, E. Longo, Journal of the European Ceramic Society 23 (2003) 707–713.
[3] T.B. Nguyen, J.P. Deloume, V. Perrichon, Applied Catalysis A: General 249 (2003) 273–284.
[4] I.T. Weber, A. Valentini, L.F.D. Probst, E. Longo, E.R. Leite, Sensors and Actuators B 97 (2004) 31–38.
[5] R. Sasikala, N.M. Gupta, S.K. Kulshreshtha, Catalysis Letters 71 (2001) 69–73.
[6] S. Mihaiu, G. Postole, M. Carata, M. Caldararu, D. Crisan, N. Dragan, M. Zaharescu, Journal of the European Ceramic Society 24 (2004) 963–967.
[7] K.C. Taylor, Catalysis Reviews: Science and Engineering 35 (1993) 457–481.
[8] A. Trovarelli, Catalysis Reviews: Science and Engineering 38 (1996) 439–520.
[9] T. Jinkawa, G. Sakai, J. Tamaki, N. Miura, N. Yamazoe, Journal of Molecular Catalysis A: Chemical 155 (2000) 193–200.

[10] P.G. Harrison, I.K. Ball, W. Azelee, W. Daniell, D. Goldfarb, Chemistry of Materials 12 (2000) 3715–3725.
[11] D. Stosica, S. Bennici, V. Rakic, A. Auroux, Catalysis Today 192 (2012) 160–168.
[12] T. Yuzhakova, V. Rakic, C. Guimon, A. Auroux, Chemistry of Materials 19 (2007) 2970–2981.
[13] T. Yuzhakova, Á. Rédey, A. Vasile, C. Hornoiu, V. Bratan, A. Utasi, J. Kovacs, Environmental Engineering and Management Journal 11 (2012) 225–230.
[14] A. Vasile, M. Caldararu, C. Hornoiu, V. Bratan, N.I. Ionescu, T. Yuzhakova, Á. Rédey, Environmental Engineering and Management Journal 11 (2012) 481–485.
[15] T. Yuzhakova, Á. Rédey, M. Caldararu, J. Kovács, G. Postole, C. Hornoiu, A. Vasile, E. Domokos, Environmental Engineering and Management Journal 8 (2009) 1403–1406.
[16] M. Caldararu, G. Postole, M. Carata, C. Hornoiu, N.I. Ionescu, T. Yuzhakova, Á. Rédey, Applied Surface Science 207 (2003) 318–326.
[17] N.I. Ionescu, M. Caldararu, Reaction Kinetics and Catalysis Letters 8 (1978) 477–481.
[18] M. Caldararu, D. Sprinceana, V.T. Popa, N.I. Ionescu, Sensors and Actuators B 30 (1996) 35–41.
[19] J.J. Fripiat, A. Jelli, G. Poncelet, J. Andre, Journal of Physical Chemistry 69 (1965) 2185–2197.
[20] A. Bielanski, M. Najbar, M. Simonska Stachura, Bulletin de l Academie Polonaise des Sciences: Serie des Sciences Chimiques 26 (1978) 249.
[21] A. Bielanski, M. Najbar, Z. Zientarski, Bulletin de l Academie Polonaise des Sciences: Serie des Sciences Chimiques 27 (1979) 417.
[22] M. Najbar, K. Stadnicka, Journal of the Chemical Society: Faraday Transactions I 79 (1983) 27.
[23] J.F. McAleer, P.T. Moseley, J.O.W. Norris, D.E. Williams, Journal of the Chemical Society: Faraday Transactions I 83 (1987) 1323–1346.
[24] R.A. Smith, Semiconductors, second ed., Cambridge University Press, Cambridge, 1978.
[25] M.K. Karanjai, D. Dasgupta, Surface and Coatings Technology 102 (1998) 73–80.
[26] M. Batzill, U. Diebold, Progress in Surface Science 79 (2005) 47–154.
[27] B.M. Reddy, A. Khan, P. Lakshmanan, M. Aouine, S. Loridant, J.C. Volta, Journal of Physical Chemistry B 109 (2005) 3355–3363.
[28] B.M. Reddy, A. Khan, Catalysis Surveys from Asia 9 (2005) 155–171.
[29] D.C. Hill, H.L. Tuller, in: R.C. Buchanan (Ed.), Ceramic Materials for Electronics, Processing, Properties and Applications, Marcel Dekker Inc., New York, 1991, pp. 249–347.
[30] M. Caldararu, G. Postole, C. Hornoiu, V. Bratan, M. Dragan, N.I. Ionescu, Applied Surface Science 181 (2001) 255–264.
[31] M. Caldararu, C. Munteanu, P. Chesler, M. Carata, C. Hornoiu, N.I. Ionescu, G. Postole, V. Bratan, Microporous and Mesoporous Materials 99 (2007) 126–131.
[32] M. Caldararu, G. Postole, M. Carata, M. Chelu, C. Hornoiu, N.I. Ionescu, T. Yuzhakova, Á. Rédey, Applied Surface Science 211 (2003) 156–165.
[33] M. Caldararu, M. Scurtu, C. Hornoiu, C. Munteanu, T. Blasco, J.M. López Nieto, Catalysis Today 155 (2010) 311–318.